Magazine of Concrete Research
Volume 67 Issue 17

Elevated temperature resistance of ultra-high-performance fibre-reinforced cementitious composites
Sobia, Hamidah, Azmi and Rafeeqi

Magazine of Concrete Research, 2015, **67**(17), 923–937
http://dx.doi.org/10.1680/macr.14.00134
Paper 1400134
Received 04/05/2014; revised 05/08/2014; accepted 13/01/2015
Published online ahead of print 07/03/2015

ice Institution of Civil Engineers
publishing

Elevated temperature resistance of ultra-high-performance fibre-reinforced cementitious composites

Anwar Q. Sobia
PhD Student, Universiti Teknologi MARA (UiTM), Malaysia
Mohd S. Hamidah
Associate Professor, Faculty of Civil Engineering, Universiti Teknologi MARA (UiTM), Malaysia
Ibrahim Azmi
Professor and Dean at Faculty of Civil Engineering, Universiti Teknologi MARA (UiTM), Malaysia
Sahibzada F. A. Rafeeqi
Professor and Pro-Vice Chancellor, NED University of Engineering and Technology, Pakistan

Elevated temperatures, specifically in the event of fire, are likely to cause extreme deterioration in fibre-reinforced polymer (FRP) strengthened reinforced concrete (RC) structures. Various types of high-performance cementitious composites (HPCC) have been explored for the protection of RC structural members against elevated temperature, but there is inadequate information in this regard for ultra-high performance fibre-reinforced cementitious composites (UHPFRCC) containing high-alumina cement (HAC) and ground granulated blast furnace slag (GGBS) in conjunction with hybrid fibres – a prospective fire-resistant UHPFRCC for structural members. In this study, the change in mechanical strength of UHPFRCC was examined before and after heat treatment, followed by thermal and microstructural analysis. Besides the control sample, three other samples containing up to 1·5% of basalt fibres, and 1 kg/m^3 of polypropylene fibres, were prepared and tested. Another mix was also prepared with only 1 kg/m^3 of polypropylene fibres. Each sample was heated to 400, 700 and 1000°C. Results showed that the use of hybrid fibres significantly improved the room temperature mechanical strengths of UHPFRCC, which were found to be 80 MPa and 14·3 MPa, respectively. However, the optimum residual compressive and flexural strength was attained by UHPFRCC with only PP fibres and hybrid fibres, respectively.

Notation

C_f compressive strength of specimen at elevated temperature at a specific curing age
C_i compressive strength of specimen at room temperature at a specific curing age
F_f flexural strength of specimen at elevated temperature at a specific curing age
F_i flexural strength of specimen at room temperature at a specific curing age
T_g glass transition temperature

Introduction

Consolidation of research studies from recent decades suggests that fibre-reinforced polymer (FRP) composite is one of the most effective retrofitting/strengthening materials for reinforced concrete (RC) structures. In addition, nowadays, this material is widely used where repair is needed because of ageing of building materials, fire/explosion, vehicle collision, earthquake or forcible modifications in the structural system by removal of columns/walls or amputation of slab openings, and also in the event of the upgrading of a building facility. This is because FRP bears lower maintenance costs, high strength-to-weight ratio and electrochemical corrosion resistance. In fact, FRP plays the role of providing an excellent alternative in restoration, rather than demolishing and then re-building RC structures, which is not always economically feasible for under-developed countries.

The behaviour of FRP has become a serious concern since its evolution and several researchers (Khalifa, 2011; Sorathia and Dapp, 1992; Ziqing, 2012) have addressed this issue in the past. It has been revealed that the FRP system becomes worse in the incident of fire and that this is principally due to the existence of epoxy in the FRP matrix having a low glass transition temperature (T_g), usually in the range of 65–150°C (Bisby *et al.*, 2005). Therefore, the only solution to enhance the fire safety of FRP-strengthened RC structures is to improve their fire resistance by providing an appropriate passive fire protection (PFP) layer. The PFP layer could help to improve the elevated temperature resistance of structural members, in the event of fire, to a level that will offer sufficient time for the inhabitants of a building to evacuate. The paramount PFP layer should be non-combustible, providing a barrier to adequately maintain the operational

temperature of FRP and structural elements in the event of fire, as well as a shield against fire spread towards adjoining buildings; above all, it should be entirely compatible with RC structural members.

Fibre-reinforced polymer strengthened RC columns (with loading) were tested (Cree *et al.*, 2012) under an ASTM E119 standard fire, insulated with cement-based PFP layers, and it was found that the FRP temperature reached the T_g of the matrix after 33 min of fire. Exposure of a FRP-strengthened RC beam with a coating of vermiculite-based cementitious insulation to the ASTM E119 fire, however, caused de-bonding of FRP within 40 min. Performance of non-cementitious materials was even worse, and the maximum ignition time of the epoxy was reported as 16·6 min with the use of phenolic coating (Sorathia and Dapp, 1992). Owing to the premier performance of cementitious composites compared with non-cementitious materials, several studies (Aydin and Baradan, 2007; Aydin, 2008; Bentz *et al.*, 2010; Cülfik and Özturan, 2002; Djaknoun *et al.*, 2012; Formosa *et al.*, 2011; Ibrahim *et al.*, 2012; Leiva *et al.*, 2005; Sarvaranta and Mikkola, 1994; Shoaib *et al.*, 2001; Wang, 2008; Won *et al.*, 2012) have been conducted in the past based on different cementitious materials. However, hybrid fibre-reinforced high-alumina cement–ground granulated blast furnace slag (HAC-GGBS) based ultra-high-performance fibre-reinforced cementitious composites (UHPFRCC) have not been well characterised at elevated temperatures.

The current paper is targeted to partially fill this gap in the existing knowledge and attempt to identify the residual mechanical properties of HAC-GGBS based UHPFRCC. HAC is selected for this study owing to its extraordinary resistance towards high temperature as well as aggressive environments. GGBS was incorporated because of its complementary effects regarding residual compressive and flexural strength of composites at high temperature in comparison to that of silica fume (Xiao and Falkner, 2006). GGBS is also added to HAC in order to suppress strength loss due to the conversion reaction under hot and humid conditions. Majumdar *et al.* (1990a) suggested a 1:1 mixture of HAC and GGBS in order to effectively counteract this conversion reaction (Majumdar and Singh, 1992). In conjunction with HAC and GGBS, different dosages (0·5%, 1%, 1·5% of the total weight of mix) of basalt fibres (BF) and a fixed amount (1 kg/m^3) of polypropylene (PP) fibres were also used in this study. Basalt fibres possess high operating temperature resistance in the range of −269–700°C (Wang *et al.*, 2011), whereas PP fibres curb the phenomenon of explosive spalling in high-performance cementitious composites (Hager and Pimienta, 2004; Ibrahim *et al.*, 2012; Khaliq and Kodur, 2013; Raivio and Sarvaranta, 1994; Wu *et al.*, 2013; Zheng *et al.*, 2014).

Experimental details

Materials

High-alumina cement is also recognised as calcium aluminate cement (CAC). Table 1 shows the chemical composition of HAC. Very fine silica sand containing 99% silicon dioxide (SiO_2) was consumed and graded according to ASTM C136-06 (ASTM, 2006). Aggregate and cement paste act like a thermal shield within UHPFRCC, therefore very fine aggregates were used in order to prevent a weak interface (Qazi *et al.*, 2012).

The chemical composition of the ground granulated blast furnace slag (GGBS) used is shown in Table 1. Physical properties of the fibres are given in Table 2. Tap water was used in all the mixes conforming to ASTM C1602/C1602M-12 (ASTM, 2012), so that it would be free from all types of silt, chloride, oil, harmful chemicals and so on.

Mix proportions

The mix proportions were proposed following a review of the literature. Later, numerous trial mixes were executed before final selection of the mix proportions. Detailed mix proportions are given in Table 3. The sand–binder ratio is the same for all mixes,

Oxides	HAC: %	GGBS: %
Silicon dioxide (SiO_2)	<6	32·9
Aluminium oxide (Al_2O_3)	38–42	14·1
Iron (III) oxide (Fe_2O_3)	13–17	—
Calcium oxide (CaO)	37–40	43·1
Magnesium oxide (MgO)	<1·5	4·8
Sulfur trioxide (SO_3)	<0·4	0·3
Titanium dioxide (TiO_2)	—	0·48
Manganese oxide (Mn_2O_3)	—	0·3
Sodium oxide (Na_2O)	—	0·16
Potassium oxide (K_2O)	—	0·27
Loss on ignition	—	1·8

Table 1. Oxide content of HAC and GGBS

Fibre type	Diameter: μm	Length: mm	Specific weight: g/cm^3	Melting point: °C	Ignition point: °C	Elastic modulus: GPa	Tensile strength: MPa	Break elongation: %	Thermal conductivity: W/m°K
Polypropylene fibres	18	6	0·91	160	360	38	400	>20	0·15
Basalt fibres	13	12·7	2·67	1450	—	100–110	4000–4300	3·15	0·031–0·038

Table 2. Physical properties of basalt and PP fibres

Mix	Total binder		PP fibre: kg/m^3	Basalt fibre: %	W/B	S/C
	HAC: %	GGBS: %				
C	50	50	0	0	0·38	0·8
CP	50	50	1	0		
CB1	50	50	1	0·5		
CB2	50	50	1	1		
CB3	50	50	1	1·5		

Note: W/B = water/binder ratio; S/C = sand/cement ratio.

Table 3. Mix proportions of UHPFRCC

at 0·8. The effect of addition of hybrid fibres, namely, PP and basalt fibres, to the mix was studied. The control mix (C) was prepared using 50% HAC and 50% GGBS. In the next mix (CP), in addition to the former materials, PP fibres were added at a rate of 1 kg/m^3 to the mix. In the subsequent mixes (CB1, CB2, CB3) basalt fibres were incorporated at three different dosages (0·5%, 1% and 1·5% of the total weight of the mix). In all of the mixes, the amounts of HAC, GGBS, sand–cement ratio, water–binder ratio and PP fibres were set to a constant value. The proposed mix proportion was derived after testing several mixes with different dosages of GGBS and comparatively low water–cement ratio (Sobia *et al.*, 2013).

Preparation of UHPFRCC

Mixing of UHPFRCC was done using a Spar high-speed mixer. First, all the dry materials were put in the mixer and mixed for about 2·5 min at slow speed (99 r/min of the planetary shaft); then, water was added to the mixture and it was further mixed for 1 min at the same speed, followed by hand mixing. Subsequently, PP fibres were added to the mixture and mixed for 1 min, followed by the addition of basalt fibres and mixing for a further 1 min at intermediate speed (176 r/min of the planetary shaft). Finally, the speed was set to the highest level (320 r/min of the planetary shaft) and mixing continued for 1·5 min.

After mixing, the casting of the specimens was carried out for each mix. For residual compressive strength and residual flexural strength testing, prism-shaped specimens of dimensions 40 mm × 40 mm × 160 mm were cast according to ASTM C348-08 (ASTM, 2008b). Specimens were cast for 28 d and 56 d of testing at room temperature and elevated temperatures for each mix. Immediately afterwards, specimens were kept in the conditioning room (details given below, in the next section). In this research room temperature was taken as 28°C.

Curing method

All specimens were kept in the conditioning room (20 ± 2°C at 60% relative humidity (RH)) for 24 h, after casting, followed by de-moulding and curing in a conventional water tank for 28 and 56 d. Specimens were kept in the conditioning room in order to keep the hydration temperature low, which could give rise to the formation of hydrogarnet (C_3AH_6) (responsible for conversion) (Fu *et al.*, 1997). In addition to that, HAC emits 2·5 times more curing heat when compared to ordinary Portland cement (OPC), which may cause cracking and strength reductions (Naus, 2006). After de-moulding, standard curing was carried out for all specimens in a water basin at an average temperature of 28°C. Curing was carried out for 28 and 56 d.

Heat treatment regime

Elevated temperatures of 400, 700 and 1000°C were adopted to expose the UHPFRCC specimens. Heating was done at the average rate of 5°C/min until it reached the target temperature and after that the target temperature was maintained for 1 h so as to attain the steady state, followed by cooling inside the furnace at an average rate of 1°C/min. A set of three prisms, at each curing age (28 and 56 d), of the specimen was exposed to elevated temperature in a gas furnace.

Methods of investigation

Residual mechanical testing

Prior to the mechanical testing, three identical specimens from each mix were weighed before and after exposure to elevated temperatures so as to calculate the average mass loss at each temperature point (400, 700 and 1000°C) with respect to their mass at room temperature. Subsequently, compressive and flexural strength testing was performed for each mix (three identical specimens each) after 28 and 56 d of curing according to ASTM C349-08 (ASTM, 2008a) and ASTM C348-08 (ASTM, 2008b), respectively. The test set-ups for compressive and flexural strength are shown in Figure 1(a) and Figure 1(b), respectively. A universal testing machine was used for testing. After each curing age, three identical specimens of each mix were exposed to the elevated temperatures of 400, 700 and 1000°C and afterwards used to calculate the residual compressive strength (RCS) and residual flexural strength (RFS), using Equation 1 and Equation 2, respectively. Before exposure to the elevated temperatures, all specimens were kept in the open atmosphere for almost 24 h in order to release excessive water. Specimens were allowed to cool down before the residual strength was determined. The following equations were used to calculate the residual compressive strength (RCS) and residual flexural strength (RFS)

$$1.\quad \text{RCS}\ (\%) = 100 - [(C_i - C_f)/C_i] \times 100$$

where C_i is the compressive strength at room temperature at the specific curing age and C_f is the compressive strength at the respective elevated temperature at the specific age

$$2.\quad \text{RFS}\ (\%) = 100 - [(F_i - F_f)/F_i] \times 100$$

where F_i is the flexural strength at room temperature at the

(a) (b)

Figure 1. Test set-up for: (a) compressive strength test; (b) flexural strength test

specific age and F_f is the flexural strength at the respective elevated temperature at the specific age.

Environmental scanning electron microscope

Environmental scanning electron microscope (ESEM) images were captured up to the magnification of 10 KX in order to examine the microstructure of UHPFRCC. The ESEM images of the specimens (C, CP and CB1) were taken before and after heat treatment.

X-ray diffraction analysis

X-ray diffraction analysis (XRD) was performed employing a Rigaku Ultima IV X-ray diffractometer, using 40 kV power and 40 mA with a Cu Kα source. XRD was executed on specimens CP and CB1, cured for 56 d and exposed to 28°C, 400°C, 700°C and 1000°C.

Differential scanning calorimetry

Differential scanning calorimetry (DSC) was performed, using an NETZSCH DSC 200 F3 apparatus, to identify the hydration products in UHPFRCC. In DSC, the samples were exposed to the heating rate of 10°C/min in a helium atmosphere. The 56 d cured UHPFRCC specimens, CP and CB1, were analysed that were exposed to 28°C, 400°C, 700°C and 1000°C.

Results and discussion

Mass loss in specimens subjected to heat treatment

Cementitious composites tend to lose their weight as the temperature elevates due to the water loss from their matrix (Zheng *et al.*, 2012). This phenomenon was also obvious in the UHPFRCC specimens. When the 28 d cured specimens were heated to 400°C (Figure 2(a)), specimen CB1 (with PP fibre + 0·5% basalt fibre) experienced the highest mass loss (11%), whereas CB2 (with PP fibre + 1% basalt fibre) showed the lowest mass loss value of 6%, which can be attributed to the evaporation of capillary water and gel water. The specimen containing PP fibres only showed a slightly greater loss in mass as compared to the control specimen, as was also experienced by Xiao and Falkner (2006). At the exposure temperature of 700°C, the highest mass loss was indicated equally by two specimens: the control and CB1, with the approximate value of 20%; the lowest value was shown by CB3 (with PP fibre + 1·5% basalt fibre) at 18·5%, owing to the loss of crystal water from the matrix. Among all exposure

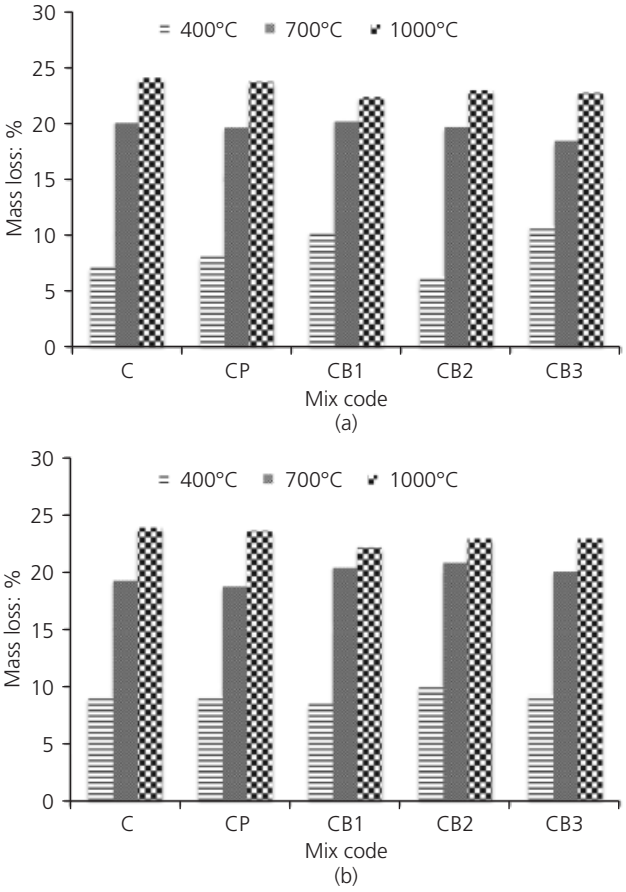

Figure 2. Mass loss in specimens subjected to heat treatment: (a) after 28 d of curing; (b) after 56 d of curing

temperatures, the highest mass loss (24%) was seen in the control specimen after heating at 1000°C. The best performance was shown by CB1, with the lowest mass loss value of 22% after exposure to 1000°C, which was also the same after 56 d of curing (Figure 2(b)). Results showed that after 700°C, mass loss of specimens remains constant and is also independent of curing ages. This also indicates that the decomposition of hydration products between 700 and 1000°C has already been completed.

Compressive strength of UHPFRCC specimens

The compressive strengths of specimens at room temperature are tabulated in Table 4. The addition of PP fibres to the control mixture caused a significant drop in the compressive strength due to the lower elastic modulus of PP fibres. However, with the addition of basalt fibre, the compressive strength was increased because of these fibres' high elastic modulus value of 89 GPa (Parnas *et al.*, 2007). Outcomes of the experiment indicated that the compressive strength of UHPFRCC (74·36 MPa) containing 1·5% of basalt fibres and 1 kg/m^3 of PP fibres was the highest among all specimens, that is 24% greater than the control specimen after 28 d of curing. In contrast, after 56 d of curing, UHPFRCC containing 1% of basalt fibres + 1 kg/m^3 of PP fibres

Mix code	Compressive strength: MPa	
	28 d	56 d
C	60·00	80·41
CP	50·60	54·91
CB1	57·97	71·59
CB2	71·40	80·49
CB3	74·36	76·05

Table 4. Measured compressive strengths of specimens at room temperature

and the control specimen were equally better than the other specimens, bearing 80·5 MPa.

The above-mentioned specimens with higher basalt fibre content showed higher strength, which might be due, first, to the good bonding of the fibres with the cementitious matrix and, second, to the good dispersion of fibres among the matrix (Butler, 2010). Overall, the entire specimens underwent an increase in compressive strength between 28 and 56 d of curing, but the control specimen exhibited the highest increase in compressive strength. The increase in compressive strength after longer curing age is corroborated by the slow reactivity of GGBS, as reported elsewhere (Fu *et al.*, 1997).

The compressive strengths of all the specimens relative to the control specimen at each temperature point are graphically shown in Figure 3. For example, compressive strength of UHPFRCC-CP (with PP fibres only) heated to 400°C was comparable with the compressive strength of the control sample heated to 400°C. It was found that after 28 d of curing (Figure 3(a)), and heating at 400°C, CB1 (with PP fibres + 0·5% basalt fibres) had the highest relative compressive strength, that is 169·86%. However, at 700°C and 1000°C, CB3 (with PP fibres + 1·5% basalt fibres) attained higher relative compressive strength values of 110% and 122%, respectively, which demonstrates the positive effect of 1·5% addition of basalt fibres to the matrix as compared to the control specimen at elevated temperature.

After 56 d of curing (Figure 3(b)), however, the relative compressive strength of CB2 (with PP fibres + 1% basalt fibres) was reported as the best among all specimens, with a value of 97·81% at the exposure of 400°C. At exposure to 700°C, the strength of CB2 (with PP fibres + 1% basalt fibres) was found to be almost equal to that of CB1 (with PP fibres + 0·5% basalt fibres), with approximately 99% of the relative compressive strength, whereas at 1000°C, only CB1 maintained the highest relative compressive strength value of 109%.

Flexural strength of UHPFRCC specimens

Table 5 lists the flexural strengths of specimens at room temperature. After 28 and 56 d of curing, CB1 (with PP fibres + 0·5%

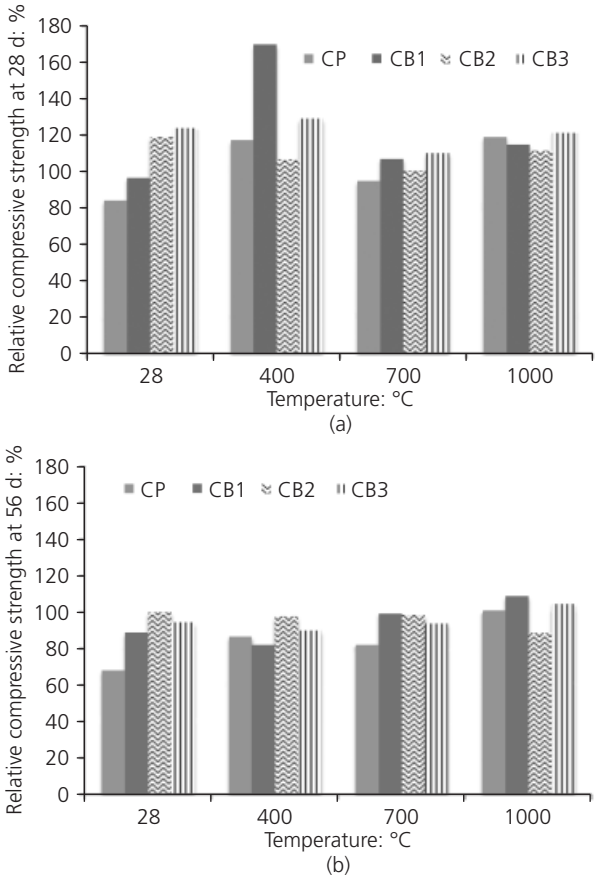

Figure 3. Relative compressive strength of specimens subjected to heat treatment after: (a) 28 d of curing; (b) 56 d of curing

Mix code	Flexural strength: MPa	
	28 d	56 d
C	8·33	7·14
CP	9·31	15·96
CB1	14·27	14·09
CB2	13·77	9·61
CB3	13·67	11·06

Table 5. Measured flexural strengths of specimens at room temperature

basalt fibres) and CP (with PP fibres only) displayed the highest flexural strength, which is substantiated by the zero effect of 0·5% of basalt fibres on PP fibre based UHPFRCC. In contrast, the control specimen showed the lowest flexural strength, a result also made clear in an earlier research study (Chu *et al.*, 2011).

In order to compare all the specimens with the control sample at each temperature point, relative flexural strength has been computed graphically, as shown in Figure 4. Figure 4(a) clearly shows that CB3 (with PP fibres + 1·5% basalt fibres) attains the best relative flexural strength of 149% and 167% at 700°C and 1000°C, respectively, after 28 d of curing. Moreover, CB1 (with PP fibres + 0·5% basalt fibres) had the significant relative flexural strength value of 177% when heated to 400°C. Furthermore, after 56 d of curing, CB2 (with PP fibres + 1% basalt fibres) showed the highest relative flexural strength values of 114% and 152% at 700°C and 1000°C, respectively. At 400°C, however, CB3 (with PP fibres + 1·5% basalt fibres) showed the highest relative flexural strength of 141% (Figure 4(b)).

Residual compressive strength

The compressive strength test was performed for both room temperature specimens (C_i) and heated specimens (CF). The formula for calculating residual compressive strength (RCS) for each mix at a specific age is given in Equation 1.

Experimental results of RCS are graphically represented in Figure 5. RCS was calculated using the formula given in Equation 1. Results show that after 28 d of curing, CB1 (with PP fibres + 0·5% basalt fibres) performed the best in the range of 28–700°C and recorded the highest RCS values of 93·34% when heated to 400°C

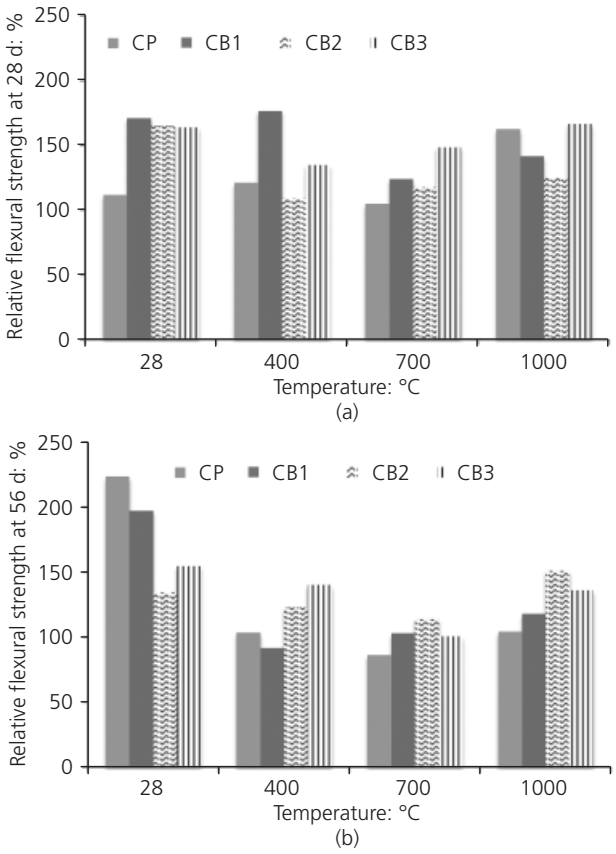

Figure 4. Relative flexural strength of specimens subjected to heat treatment after: (a) 28 d of curing; (b) 56 d of curing

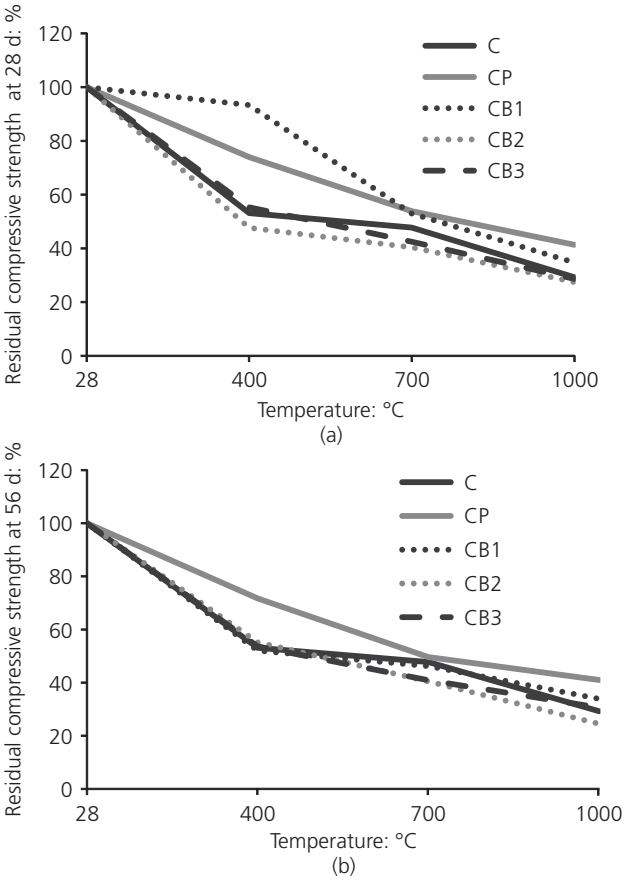

Figure 5. Residual compressive strength of specimens subjected to heat treatment after: (a) 28 d of curing; (b) 56 d of curing

and 52·96% at 700°C (almost equal to UHPFRCC with PP fibre only). However, afterwards there was a significant drop in RCS value of CB1 (with PP fibres + 0·5% basalt fibres) in comparison with the CP (with PP fibre only) specimen. Finally, CP showed the lowest strength drop in the range of 700–1000°C, with the highest RCS value of 41·31% at 1000°C. This may be due to the melting of PP fibres in the UHPFRCC, which leaves behind micro-channels to mitigate the vapour tension in the capillaries, resulting in improved residual compressive strength (Chen and Liu, 2004). Overall the lowest performance was shown by CB2 (with PP fibres + 1% basalt fibres) after both 28 and 56 d of curing. The quasi-linear decrease in the RCS, at temperatures higher than 400°C, might be interpreted as due to the removal of bound water from the specimen.

After 56 d of curing, CP possessed highest RCS value at all temperature ranges as compared to the other mixes. However, among basalt fibre specimens, CB1 produced the highest RCS value at both curing ages. The reason behind the poor RCS value of specimens containing more than 0·5% of basalt fibres could be attributed to the congestion of fibres, which blocked the moisture-release path created by PP fibres, resulting in thermal cracking owing to pore pressure development.

Residual flexural strength

The residual flexural strength (RFS) was computed using the flexural strength readings of unheated (F_i) and heated specimens (F_f). RFS of specimens was calculated using Equation 2.

Laboratory results show that after 28 d of curing (Figure 6(a)) CP performed well throughout the elevated temperature exposure as compared to other specimens, with 39·08% RFS value at 1000°C. On the other hand, at the exposure of 700°C RFS of the control specimen was only 6% better than CP, an almost negligible improvement. The lowest RFS value was exhibited by CB1 (with PP fibres + 0·5% basalt fibres) and CB2 (with PP fibres + 1% basalt fibres), that is approximately 19% less than the CP specimen; this may be because the glass transition temperature of basalt fibre was reached at around 673°C (Wang *et al.*, 2012), which made the specimens less effective at elevated temperature beyond 1000°C.

Figure 6(b) illustrates the RFS value of specimens after exposure to elevated temperature after 56 d of curing. UHPFRCC containing 1% of basalt fibres (CB2) recorded the best RFS value of 49%, which is 18% better than the control sample (C). The better performance of CB2 may affirm that even though basalt fibres

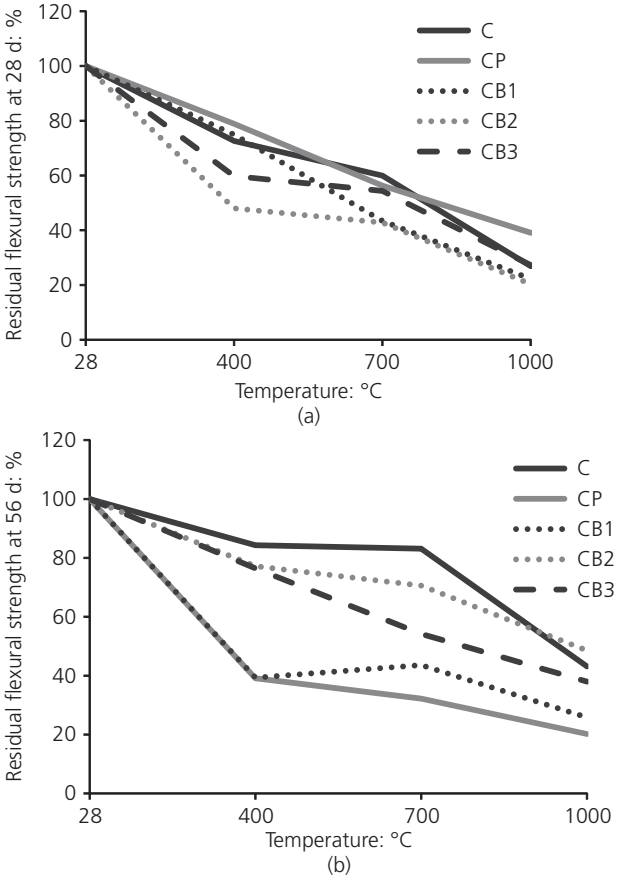

Figure 6. Residual flexural strength of specimens subjected to heat treatment after after: (a) 28 d of curing; (b) 56 d of curing

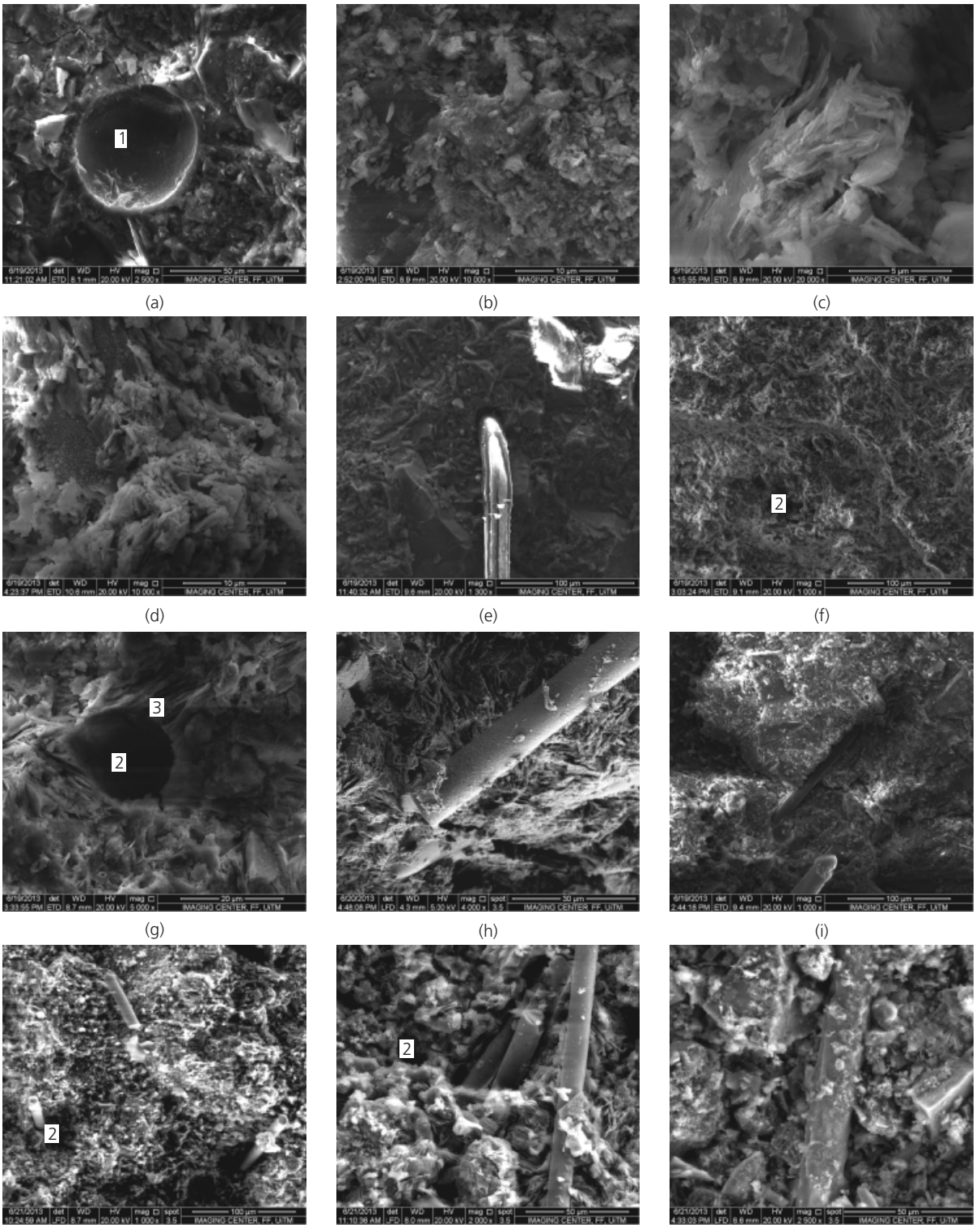

Figure 7. ESEM images of control, PP fibre and PP fibre + basalt fibre containing specimens at different temperature exposures after 56 d of curing: (a) control specimen at 28°C; (b) control specimen at 400°C; (c) control specimen at 700°C; (d) control specimen at 1000°C; (e) PP fibre specimen at 28°C; (f) PP fibre specimen at 400°C; (g) PP fibre specimen at 700°C; (h) PP fibre specimen at 1000°C; (i) PP + 0·5% basalt fibre specimen at 28°C; (j) PP + 0·5% basalt fibre specimen at 400°C; (k) PP + 0·5% basalt fibre at 700°C; (l) PP + 0·5% basalt fibre specimen at 1000°C

have reached their glass transition temperature beyond 673°C (Wang *et al.*, 2012), resulting in the weakening of the matrix, that feebleness of the matrix may be compensated by the improved reactivity of GGBS after 56 d of curing. Specimen CP performed the least well after 56 d of curing, unlike the result found at 28 d of curing.

Environmental scanning electron microscopy

The ESEM images of the specimens (C, CP and CB1) before and after heat treatment are shown in Figure 7. Mono calcium aluminate (CA) is the key constituent in all HACs. A series of calcium aluminate hydrates are formed when mono calcium aluminate reacts with water. In the presence of GGBS, HAC also reacts with amorphous silica present in GGBS to form strätlingite (Heikal *et al.*, 2004). The ESEM of samples at room temperature (Figures 7(a), 7(e) and 7(i)) shows the dark and dense microstructure that can be attributed to the presence of strätlingite, as also verified by thermal analysis and XRD (as explained in the following two sections). In the control sample, point 1 indicates that a silica particle from GGBS has reacted with monocalcium aluminate hydrate (CAH_{10}) to produce strätlingite (Bushnell-Watson and Sharp, 1992; Midgley and Rao, 1978) by the following reaction

$$\text{I.} \quad 2CAH_{10} + S \rightarrow C_2ASH_8 + AH_3 + 9H$$

As a consequence of exposure to elevated temperatures, distinct changes in morphology occurred. After exposure to 400°C, along with the dense, dark microstructure, a light colour appeared which shows the parallel conversion of strätlingite into gehlenite (C_2AS) by the following reaction (Mostafa *et al.*, 2012)

$$\text{II.} \quad C_2ASH_8 \rightarrow C_2AS + 8H$$

Point 2, as marked in the ESEM images, shows the melting of PP fibres, providing a channel for the release of steam. PP fibres melt at approximately 162°C (324°F), which helps to induce porosity in UHPFRCC through which pore pressure is alleviated, with associated reduced degradation to the microstructure (Khaliq and Kodur, 2013). It is also important to note that, even after the

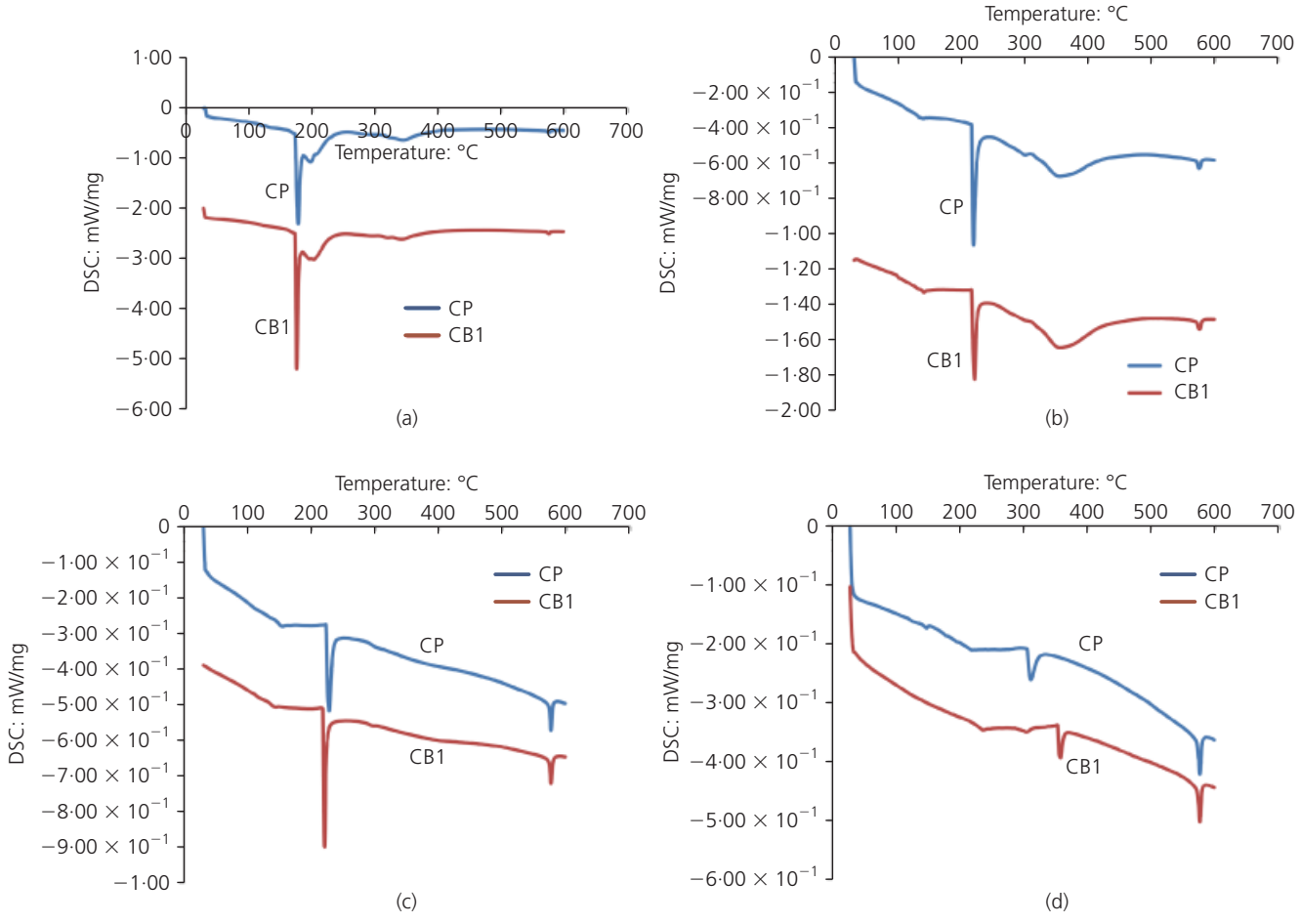

Figure 8. DSC thermograms for the specimens after exposure to: (a) 28°C; (b) 400°C; (c) 700°C; (d) 1000°C

exposure of samples at 1000°C, PP fibres were detected in the samples, which shows that within a certain depth of sample the temperature did not rise beyond 162°C (melting point of PP fibre). This is an indication of the good thermal resistance of the matrix.

Differential scanning calorimetry

The DSC thermograms of the hydrated UHPFRCC specimens (CP and CB1) cured for 56 d are shown in Figure 8. The figure shows the DSC curves of specimens containing only PP fibres (CP), as well as the specimen with hybrid fibres (1% PP fibre+0·5% basalt fibre), CB1, exposed to room temperature as well as elevated temperatures.

The first peak (Figure 8(a)) at 180°C shows the decomposition of strätlingite (C_2ASH_8), followed by a small shoulder probably due to the dehydration of dicalcium aluminium hydrate (C_2AH_8). At the same position the peak is sharper in CB1 as compared to CP, which explains the large quantity of strätlingite leading to the high strength of CB1 at room temperature. Formation of strätlingite leads to the greater strength (Majumdar and Singh, 1992). The shallow depression at 350°C indicates the presence of hydrogarnet (C_3AH_6) which is at a considerably lower amount. The peak at 210°C (Figure 8(b)) shows the presence of strätlingite. The small peak at around 300°C indicates gibbsite (AH_3) followed by the broad depression around 350°C, which might be due to the dehydration of a member of the hydrogarnet series, $C_3AS_3 - {}_XH_{2X}$, where $X = 0$–3 (Hidalgo *et al.*, 2009). Alumina trihydrate crystals were detected in Figure 11 (point 5) After the treatment of the specimen at 700°C (Figure 8(c)), only two significant peaks persist at 220°C and 590°C, which are ascertained to be either dicalcium aluminium hydrate or carboaluminate hydrate (Bushnell-Watson and Sharp, 1985) and quartz,

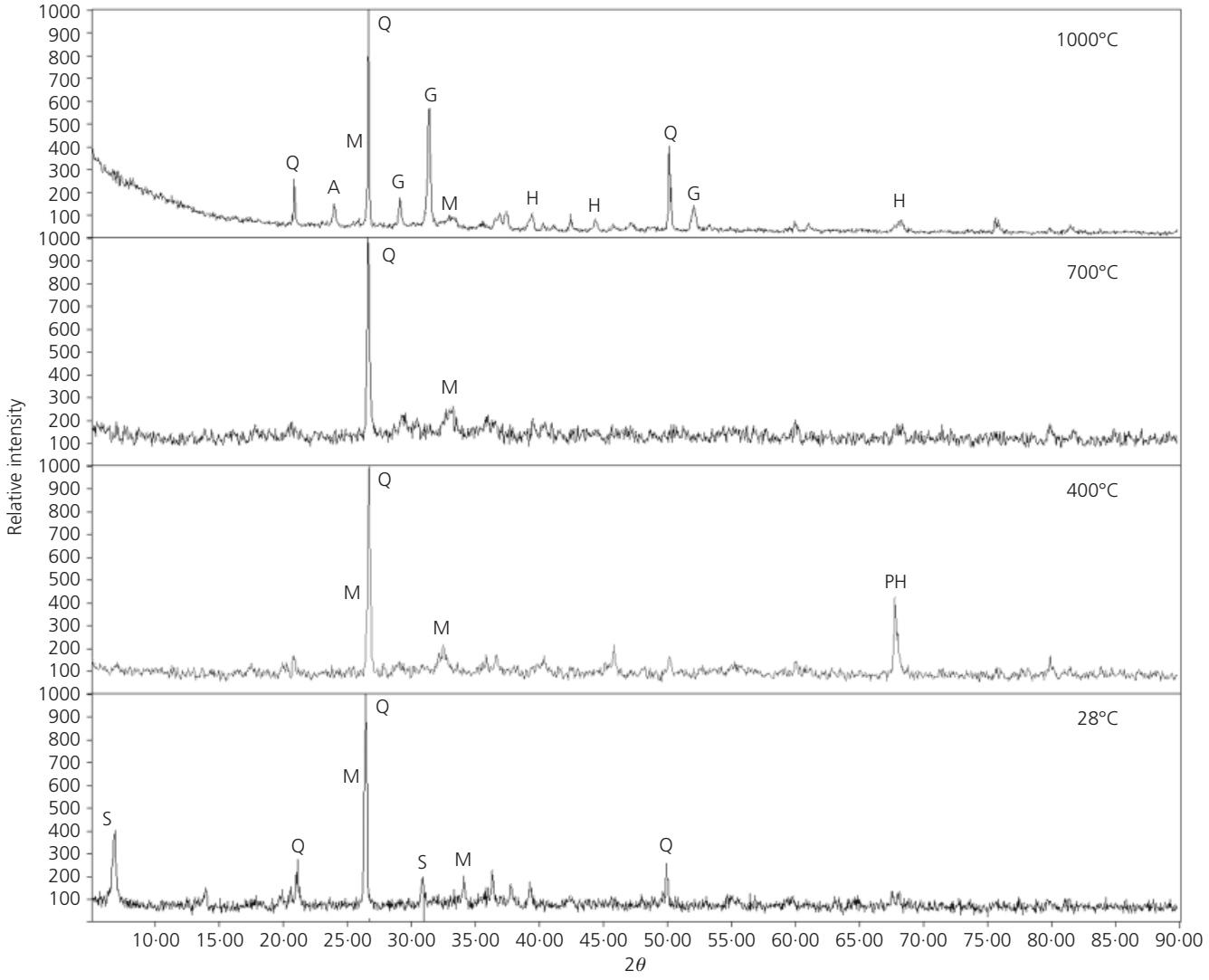

Figure 9. ESEM of sample CB1 exposed to 400°C showing hydration products. S: strätlingite; Q: quartz; M: mullite; G: gehlenite; H: hydrogarnet; Ma: mayanite

respectively. Well-oriented blades (or plates) of strätlingite can also be seen in Figure 7(g), at point 3. Continuous detection of strätlingite at elevated temperature shows that the reactivity of GGBS progressively increased, resulting in the release of silica, which in turn reacts with dicalcium aluminium hydrate to produce strätlingite (Ding *et al.*, 1996). After the exposure of samples to 1000°C, only hydrogarnet and quartz remained in both samples, CP and CB1.

With all of the exposure temperatures, samples show the peak around 570–590°C, which is due to the allotropic transformation of quartz, $SiO_2\alpha$ to $SiO_2\beta$, as was also found by Sdiri *et al.* (2010). This transformation is a reversible process, so it could be supposed that quartz-α reformed after cooling, once the thermal treatment finished (Fares *et al.*, 2010). Presence of quartz (SiO_2) in the samples, even after exposure to 1000°C, is an indication that the overall temperature of the specimen did not increase beyond 800°C, because the disintegration of silica sand occurs at 800°C. The presence of quartz in both of the samples has also been confirmed by their XRD patterns (Figure 10 and Figure 11).

X-ray diffraction analysis

Figure 10 and Figure 11 depict the XRD patterns of samples CP and CB1 cured for 56 d and exposed to different temperatures. At 28°C, strätlingite is present at a greater amount in CP as compared to CB1, a result that is also verified by the DSC thermogram of the same samples (Figure 8). Mullite is also traced throughout in both samples, which is a promising coating material due to its high thermal resistance and low thermal conductivity (Arizmendi-Morquecho *et al.*, 2012). Mullite is a stable phase, which occurs in refractory materials (Pollmann, 2012). Mullite crystals were also detected in the ESEM of the

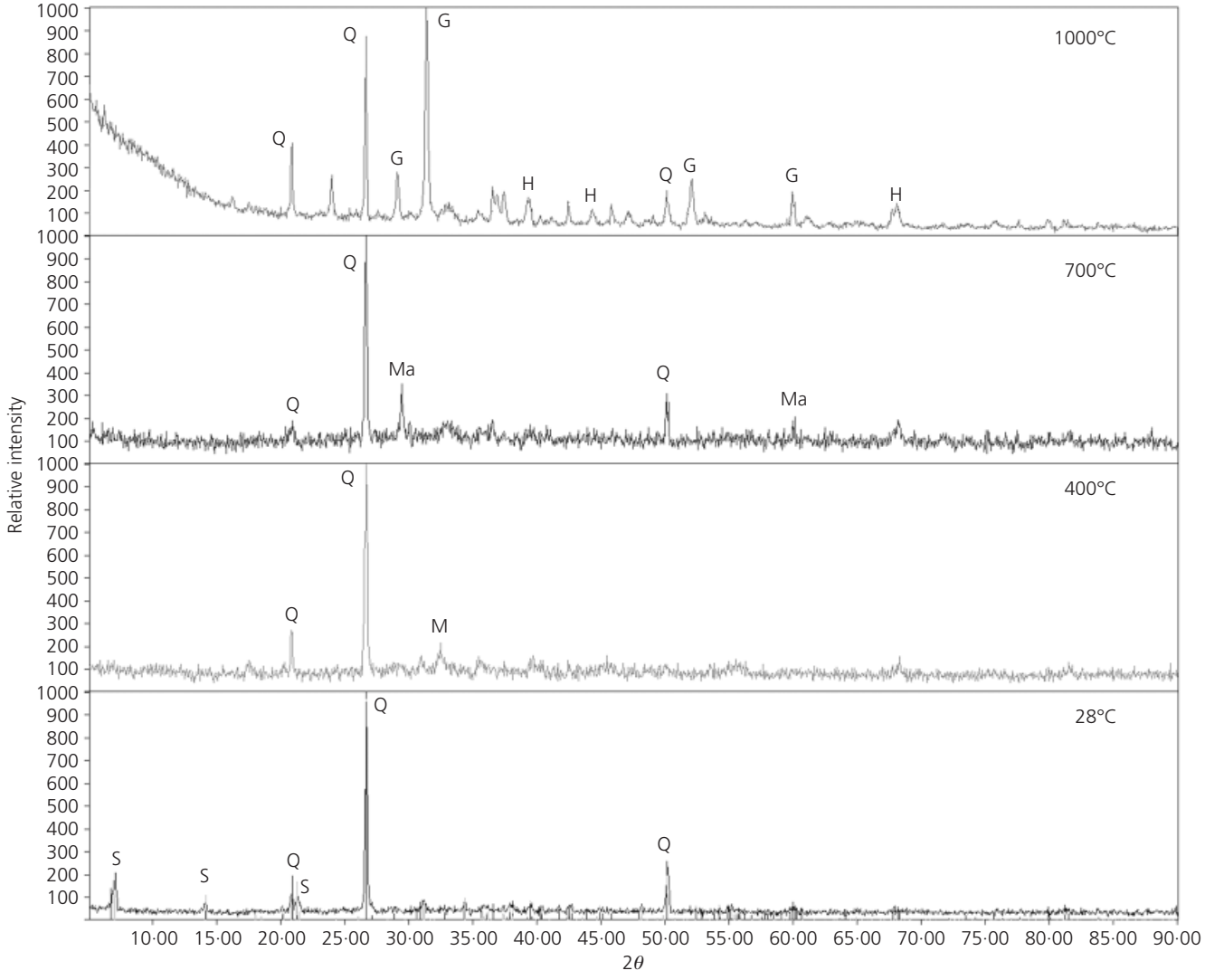

Figure 10. XRD pattern of samples containing PP fibres (CP) subjected to different temperatures. S: strätlingite; Q: quartz; M: mullite; G: gehlenite; H: hydrogarnet; Ma: mayanite

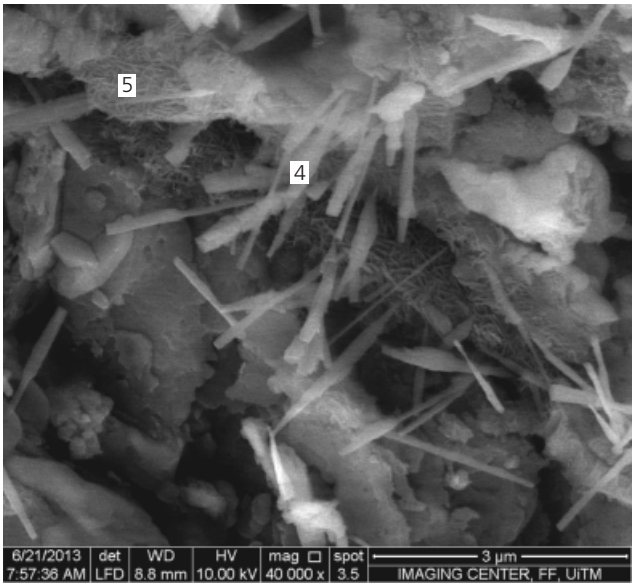

Figure 11. XRD pattern of samples containing PP + 0·5% basalt fibres (CB1) subjected to different temperatures

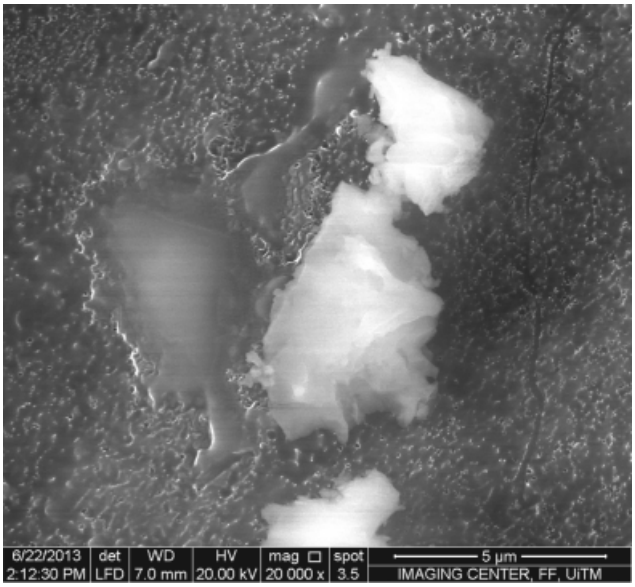

Figure 12. ESEM of sample exposed to 1000°C showing ceramic microstructure

sample as shown in Figure 11 (point 4). Hydrogarnet was not detected in the samples tested at room temperature, which clearly indicates the effectiveness of GGBS in curbing the conversion reaction. This is further explained in a past study (Majumdar *et al.*, 1990b) showing strätlingite is a product of hydrogarnet (C_3AH_6, a conversion product of HAC) and silica (SiO_2) in GGBS. With the progress of this reaction, C_3AH_6 vanishes and definitely hinders the strength reduction in HAC-based UHPFRCC. An amorphous phase is also produced in substantial quantities (Edmonds and Majumdar, 1988). This amorphous phase is mostly identified as alumina gel; however, it has been claimed that this must be a calcium–aluminate–hydrate (C-A-H) phase, calcium aluminate hydrate of unknown composition (Payne and Sharp, 1989).

Gehlenite is detected in both samples after being heated to 1000°C; this is a main ceramic mineral and imparts strength and high-temperature resistance to the composite (Aydin and Baradan, 2007). The microstructure of gehlenite is shown in Figure 12. Specimen CB1 contained the greatest amount of gehlenite, resulting in a greater relative compressive strength as compared to CP after 56 d of curing (Figure 3(b)).

At elevated temperature, hexagonal calcium aluminates (such as monocalcium aluminate hydrate (CAH_{10}) and dicalcium aluminate hydrate (C_2AH_8)) are converted into a stable cubic hydrogarnet phase (Mostafa *et al.*, 2012), as is also found in the XRD patterns of samples heated to 1000°C. Hydrogarnet bears a very stable and durable structure, even at much higher temperatures (Macdowell, 1989), but it makes the microstructure porous, which remarkably reduces the mechanical strength (Mostafa *et al.*, 2012), as shown in the ESEM image of samples heated to 1000°C (see Figure 7(d)).

Conclusions

The following conclusions could be made on the basis of the experimental results.

- Mass loss was found to be significant between 400°C and 700°C for all UHPFRCC specimens. However, the lowest mass loss was experienced by the UHPFRCC (CB2) containing hybrid fibres (1 kg/m^3 of PP fibres + 1% of basalt fibres).
- After exposure to 1000°C, the UHPFRCC containing PP fibres (CP) showed the best performance, equally after 28 and 56 d of curing, that is 41%, in comparison to those tested at room temperature.
- UHPFRCC cured for 28 d and containing PP fibres (CP) showed the highest flexural strength of 39% after heating at 1000°C, whereas the UHPRFCC (CB2) with hybrid fibres (1 kg/m^3 of PP fibres + 1% of basalt fibres) exhibited the best residual flexural strength of 48·5% after 56 d of curing.
- At room temperature, all specimens experienced an increase in compressive strength after 56 d of curing, as compared to 28 d of curing. The highest room temperature compressive strength (80 MPa) was shown by the hybrid fibre based UHPFRCC-CB1 (1 kg/m^3 of PP fibres + 0·5% of basalt fibres) after 56 d of curing. The highest room temperature flexural strength was attained by UHPFRCC-CP (15·96 MPa), containing only PP fibres, after 56 d of curing.
- Thermal and microstructural analyses showed that the superior performance of UHPFRCC may be attributed to the formation of high-temperature-resistant phases, including gehlenite and mullite, which also imparted a ceramic-type microstructure at elevated temperature up to 1000°C.

In conclusion, the use of combined HAC/GGBS and the inclusion of hybrid fibres (PP + basalt fibres) can produce a UHPFRCC that offers good mechanical properties as well as improved resistance against thermal load up to 1000°C, as compared to normal Portland cement based composites. Such UHPFRCC is a promising environmentally friendly fire protection material for FRP-strengthened RC structures.

Acknowledgements

The authors gratefully acknowledge the help of Universiti Teknologi MARA (UiTM) and NED University of Engineering and Technology (NEDUET) for offering all the research facilities necessary for the present investigation. YTL Cement, Kamenney vek and Maccaferri, who provided GGBS, basalt fibres and polypropylene fibres, respectively, for the experimental work, are also acknowledged. In particular, the authors would also like to acknowledge the faculty for the future programme, Ministry of Higher Education Malaysia, ERGS grant number 600-RMI/ERGS 5/3 (22/2012) and 600-RMI/DANA5/3 CIFI(26/2013) for providing the necessary financial support to conduct this research.

REFERENCES

Arizmendi-Morquecho A, Chávez-Valdez A and Alvarez-Quintana J (2012) High temperature thermal barrier coatings from recycled fly ash cenospheres. *Applied Thermal Engineering* **48**: 117–121, http://dx.doi.org/10.1016/j.applthermaleng.2012.05.004.

ASTM (2006) ASTM C136-06: Standard test method for sieve analysis of fine and coarse aggregates. ASTM International, West Conshohocken, PA, USA.

ASTM (2008a) ASTM C349-08: Standard test method for compressive strength of hydraulic-cement mortars (using portions of prisms broken in flexure). ASTM International, West Conshohocken, PA, USA.

ASTM (2008b) ASTM C348-08: Standard test method for flexural strength of hydraulic-cement mortars. ASTM International, West Conshohocken, PA, USA.

ASTM (2012) ASTM C1602/C1602M-12: Standard specific cation for mixing water used in the production of hydraulic cement concrete. ASTM International, West Conshohocken, PA, USA.

Aydin S (2008) Development of a high-temperature-resistant mortar by using slag and pumice. *Fire Safety Journal* **43(8)**: 610–617.

Aydin S and Baradan B (2007) Effect of pumice and fly ash incorporation on high temperature resistance of cement based mortars. *Cement and Concrete Research* **37(6)**: 988–995.

Bentz D, Peltz M, Duran-Herrera A *et al.* (2010) Thermal properties of high-volume fly ash mortars and concretes. *Journal of Building Physics* **34(263)**: 275–275.

Bisby LA, Kodur VKR and Green MF (2005) Fire endurance of fiber-reinforced polymer-confined concrete columns. *ACI Structural Journal* **102(6)**: 883–891.

Bushnell-Watson S and Sharp J (1985) The detection of the carboaluminate phase in hydrated high alumina cements by differential thermal analysis. *Thermochimica Acta* **93**: 613–616.

Bushnell-Watson SM and Sharp JH (1992) The application of thermal analysis to the hydration and conversión reactions of calcium alumínate cements. *Materiales de Construcción* **42(228)**: 13–32.

Butler M (2010) *Report of Material Testing on Basalt Fibres 4 Series 1a: Basic Material Properties of Cement Mortar with 3 Types of Basalt Fibres with Length of 6 mm*. Fakultät Bauingenieurwesen, Institut für Baustoffe, Arbeitsgruppe Baustofftechnik, Moscow, Russia.

Chen B and Liu J (2004) Residual strength of hybrid-fiber-reinforced high-strength concrete after exposure to high temperatures. *Cement and Concrete Research* **34(6)**: 1065–1069, http://dx.doi.org/10.1016/j.cemconres.2003.11.010.

Chu FJ, Liu HW, Yang ZB and Dai HM (2011) Bending performance of basalt fiber reinforced cement. *Advanced Materials Research* **332–334**: 2142–2145, http://dx.doi.org/10.4028/www.scientific.net/AMR.332–334.2142.

Cree D, Chowdhury EU, Green MF *et al.* (2012) Performance in fire of frp-strengthened and insulated reinforced concrete columns. *Fire Safety Journal* **54**: 86–95, http://dx.doi.org/10.1016/j.firesaf.2012.08.006.

Cülfik MS and Özturan T (2002) Effect of elevated temperatures on the residual mechanical properties of high-performance mortar. *Cement and Concrete Research* **32(5)**: 809–816.

Ding J, Fu Y and Beaudoin J (1996) Study of hydration mechanisms in the high alumina cement–sodium silicate system. *Cement and Concrete research* **26(5)**: 799–804.

Djaknoun S, Ouedraogo E and Ahmed Benyahia A (2012) Characterisation of the behaviour of high performance mortar subjected to high temperatures. *Construction and Building Materials* **28(1)**: 176–186.

Edmonds R and Majumdar A (1988) The hydration of monocalcium aluminate at different temperatures. *Cement and Concrete Research* **18(2)**: 311–320.

Fares H, Remond S, Noumowe A and Cousture A (2010) High temperature behaviour of self-consolidating concrete. *Cement and Concrete Research* **40(3)**: 488–496, http://dx.doi.org/10.1016/j.cemconres.2009.10.006.

Formosa J, Chimenos JM, Lacasta AM *et al.* (2011) Novel fire-protecting mortars formulated with magnesium by-products. *Cement and Concrete Research* **41(2)**: 191–196.

Fu Y, Ding F and Beaudoin J (1997) Temperature dependence of compressive strength of conversion-inhibited high alumina cement concrete. *ACI Materials Journal* **94(6)**: 540–544.

Hager I and Pimienta P (2004) The impact of the addition of polypropylene fibres on the mechanical properties of high performance concretes exposed to high temperatures. *Proceedings of the 6th Rilem Symposium on Fibre-Reinforced Concretes (FRC), Varenna, Italy*, pp. 575–582.

Heikal M, Radwan MM and Morsy MS (2004) Influence of curing temperature on the physico-mechanical, characteristics of calcium aluminate cement with air cooled slag or water cooled slag. *Ceramics-Silikáty* **48(4)**: 185–196.

Hidalgo A, García JL, Alonso MC *et al.* (2009) Microstructure development in mixes of calcium aluminate cement with silica fume or fly ash. *Journal of Thermal Analysis and Calorimetry* **96(2)**: 335–345, http://dx.doi.org/10.1007/s10973–007–8439–3.

Ibrahim RK, Hamid R and Taha MR (2012) Fire resistance of high-volume fly ash mortars with nanosilica addition. *Construction and Building Materials* **36**: 779–786, http://dx.doi.org/10.1016/j.conbuildmat.2012.05.028.

Khalifa T (2011) *The Effects of Elevated Temperatures on Fibre Reinforced Polymers for Strengthening Concrete*. Master of Applied Science thesis, Queen's University Kingston, Ontario, Canada.

Khaliq W and Kodur V (2013) High temperature mechanical properties of high-strength fly ash concrete with and without fibers. *ACI Materials Journal* **109(6)**: 665–674.

Leiva C, Vilches L, Vale J and Fernandezpereira C (2005) Influence of the type of ash on the fire resistance characteristics of ash-enriched mortars. *Fuel* **84(11)**: 1433–1439.

Macdowell JF (1989) Stratlingite and hydrogarnet from calcium aluminosilicate glass cements. *Materials Research Society Symposium Proceedings*, pp. 159–179.

Majumdar AJ and Singh B (1992) Properties of some blended high-alumina cements. *Cement and Concrete Research* **22(4)**: 1101–1114.

Majumdar A, Edmonds R and Singh B (1990a) Hydration of secar 71 aluminous cement in presence of granulated blast furnace slag. *Cement and Concrete Research* **20(1)**: 7–14.

Majumdar AJ, Singh B and Edmonds RN (1990b) Hydration of mixtures of 'ciment fondu' aluminous cement and granulated blast furnace slag. *Cement and Concrete Research* **20(2)**: 197–208.

Midgley HG and Rao PB (1978) Formation of stratlingite, $2CaO.SiO_2.Al_2O_3.8H_2O$, in relation to the hydration of high alumina cement. *Cement and Concrete Research* **8(2)**: 169–172, http://dx.doi.org/10.1016/0008–8846(78)90005–4.

Mostafa NY, Zaki ZI and Elkader OHA (2012) Chemical activation of calcium aluminate cement composites cured at elevated temperature. *Cement and Concrete Composites* **34(10)**: 1187–1193.

Naus DJ (2006) *The Effect of Elevated Temperature on Concrete Materials and Structures –A Literature Review.* Oak Ridge National Labortary, Washington, DC, USA.

Parnas R, Shaw MT and Liu Q (2007) *Basalt Fiber Reinforced Polymer Composites*. Institute of Materials Science, University of Connecticut, Connecticut, USA.

Payne DR and Sharp JH (1989) The nature of the gel phase in calcium aluminate cements. *The Microstructure and Chemistry of Cement and Concrete, Abstract at Institute of Ceramics Conference, University of Aberdeen*.

Pollmann H (2012) Calcium aluminate cements-raw materials, differences, hydration and properties. *Reviews in Mineralogy and Geochemistry* **74(1)**: 1–82, http://dx.doi.org/10.2138/rmg.2012.74.1.

Qazi S, Hamidah MS, Ibrahim A *et al.* (2012) State-of-the-art review-behaviour of thin high performance cementitious composites (THPCC) at elevated temperatures. *Proceedings of the 11th International Conference on Concrete Engineering and Technology 2012 (CONCET2012), Putrajaya, Malaysia*.

Raivio P and Sarvaranta L (1994) Microstructure of fibre mortar composites under fire impact-effect of polypropylene and polyacrylonitrile fibres. *Cement and Concrete Research* **24(5)**: 896–906.

Sarvaranta L and Mikkola E (1994) Fibre mortar composites under fire conditions: effects of ageing and moisture content of specimens. *Materials and Structures* **27(9)**: 532–538.

Sdiri A, Higashi T, Bouaziz S and Benzina M (2010) Synthesis and characterization of silica gel from siliceous sands of southern Tunisia. *Arabian Journal of Chemistry* **7(4)**: 486–493, http://dx.doi.org/10.1016/j.arabjc.2010.11.007.

Shoaib MM, Ahmed SA and Balaha MM (2001) Effect of fire and cooling mode on the properties of slag mortars. *Cement and Concrete Research* **31(11)**: 1533–1538.

Sobia AQ, Shyzleen A, Hamidah MS *et al.* (2013) *Post elevated Temperature Effect on the Strength and Microstructure of Thin High Performance Cementitious Composites (THPCC)*. World Academy of Science, Engineering and Technology, Kuala Lumpur, Malaysia.

Sorathia U and Dapp T (1992) Fire performance of composites. *Materials Engineering* **1992(September)**: 10.

Wang H (2008) The effects of elevated temperature on cement paste containing ggbfs. *Cement and Concrete Composites* **30(10)**: 992–999.

Wang HL, Yang XL, Ren QC and Dong P (2011) Research progress basalt fiber in civil engineering. *Applied Mechanics and Materials* **71–78**: 1484–1487, http://dx.doi.org/10.4028/www.scientific.net/AMM.71–78.1484.

Wang N, Hou S and Jin HY (2012) Crystallization behavior of heat-treated basalt fiber. *Advanced Materials Research* **560–561**: 3–7, http://dx.doi.org/10.4028/www.scientific.net/AMR.560–561.3.

Won JP, Kang HB, Lee SJ and Kang JW (2012) Eco-friendly fireproof high-strength polymer cementitious composites. *Construction and Building Materials* **30**: 406–412, http://dx.doi.org/10.1016/j.conbuildmat.2011.12.034.

Wu X, Wu Z-m, Zheng J-j *et al.* (2013) An experimental study on the performance of self-compacting lightweight concrete exposed to elevated temperature. *Magazine of Concrete Research* **65(13)**: 780–786, http://dx.doi.org/10.1680/macr.12.00218.

Xiao J and Falkner H (2006) On residual strength of high-performance concrete with and without polypropylene fibres at elevated temperatures. *Fire Safety Journal* **41(2)**: 115–121, http://dx.doi.org/10.1016/j.firesaf.2005.11.004.

Zheng W, Li H and Wang Y (2012) Compressive behaviour of hybrid fiber-reinforced reactive powder concrete after high temperature. *Materials and Design* **41**: 403–409, http://dx.doi.org/10.1016/j.matdes.2012.05.026.

Zheng W, Luo B and Wang Y (2014) Microstructure and mechanical properties of RPC containing PP fibres at elevated temperatures. *Magazine of Concrete Research* **66(08)**: 397–408.

Ziqing Y (2012) *Thermal and mechanical responses of fiber reinforced polymer composites under one-sided fire exposure*. PhD thesis, Mechanical Engineering, The University of North Carolina, Chapel Hill, NC, USA.